Article

Developmental Cell

Migration of Founder Epithelial Cells Drives Proper Molar Tooth Positioning and Morphogenesis

Graphical Abstract

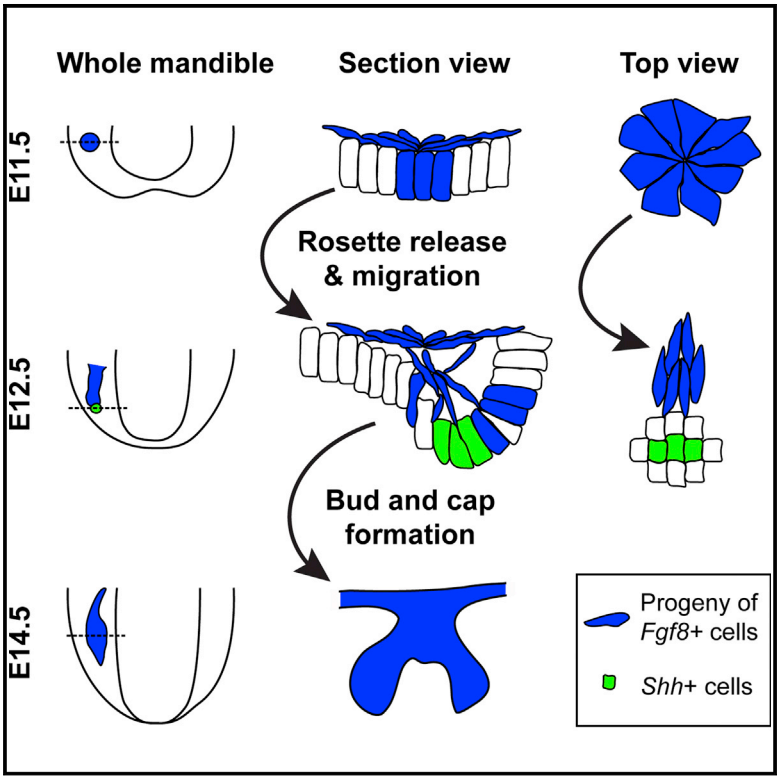

Authors

Jan Prochazka, Michaela Prochazkova, Wen Du, ..., John L. Rubenstein, Torsten Wittmann, Ophir D. Klein

Correspondence

ophir.klein@ucsf.edu

In Brief

Prochazka et al. investigate mechanisms of organ positioning using the tooth as a model. Combining lineage tracing, genetic cell ablation, and confocal live imaging, they identified a *Fgf8*-expressing epithelial cell population whose migration toward a *Shh*-expressing region in the mandible, the tooth placode initiation site, is required for tooth development.

Highlights

- Migratory *Fgf8*-expressing cells are the founding population during tooth development
- Intraepithelial migration is essential for proper positioning of the molar primordium
- *Shh* serves as a guidance signal for migratory cells in the developing tooth

Prochazka et al., 2015, Developmental Cell *35*, 713–724
December 21, 2015 ©2015 Elsevier Inc.
http://dx.doi.org/10.1016/j.devcel.2015.11.025

Developmental Cell
Article

Migration of Founder Epithelial Cells Drives Proper Molar Tooth Positioning and Morphogenesis

Jan Prochazka,[1,2] Michaela Prochazkova,[1,2] Wen Du,[1,3] Frantisek Spoutil,[2] Jolana Tureckova,[2] Renee Hoch,[4] Tomomi Shimogori,[5] Radislav Sedlacek,[2] John L. Rubenstein,[4] Torsten Wittmann,[6] and Ophir D. Klein[1,7,*]
[1]Department of Orofacial Sciences and Program in Craniofacial Biology, University of California, San Francisco, 513 Parnassus Avenue, San Francisco, CA 94143, USA
[2]Laboratory of Transgenic Models of Diseases, Institute of Molecular Genetics of the ASCR, v.v.i., Prague 4 14220, Czech Republic
[3]State Key Laboratory of Oral Diseases, West China Hospital of Stomatology, Sichuan University, Chengdu, Sichuan 610041, China
[4]Department of Psychiatry, Nina Ireland Laboratory of Developmental Neurobiology, University of California, San Francisco, 1500 4th Street, San Francisco, CA 94143, USA
[5]Laboratory for Molecular Mechanisms of Thalamus Development, RIKEN Brain Science Institute, 2-1 Hirosawa Wako, Saitama 351-0198, Japan
[6]Department of Cell and Tissue Biology, University of California, San Francisco, 513 Parnassus Avenue, San Francisco, CA 94143, USA
[7]Department of Pediatrics and Institute for Human Genetics, University of California, San Francisco, 513 Parnassus Avenue, San Francisco, CA 94143, USA
*Correspondence: ophir.klein@ucsf.edu
http://dx.doi.org/10.1016/j.devcel.2015.11.025

SUMMARY

The proper positioning of organs during development is essential, yet little is known about the regulation of this process in mammals. Using murine tooth development as a model, we have found that cell migration plays a central role in positioning of the organ primordium. By combining lineage tracing, genetic cell ablation, and confocal live imaging, we identified a migratory population of *Fgf8*-expressing epithelial cells in the embryonic mandible. These *Fgf8*-expressing progenitors furnish the epithelial cells required for tooth development, and the progenitor population migrates toward a *Shh*-expressing region in the mandible, where the tooth placode will initiate. Inhibition of Fgf and Shh signaling disrupted the oriented migration of cells, leading to a failure of tooth development. These results demonstrate the importance of intraepithelial cell migration in proper positioning of an initiating organ.

INTRODUCTION

The precise positioning of developing organs is essential for proper embryogenesis, but the mechanisms that facilitate this process at a cellular level are not well understood. Morphogen gradients have classically been invoked as regulators of organ positioning (Wolpert, 1969), but how such signaling events are translated into cellular behaviors remains elusive. One important mechanism of organ positioning that has been reported in some vertebrates, but not yet well-studied in mammals, involves epithelial migration, which regulates patterning of mechanosensory organs in the lateral line of fish. In this process, founder epithelial cells form rosettes, migrate in an anteroposterior direction, and establish primordia of individual organs; such events are often mediated by Fgf, Wnt, and chemokine signaling (Nechiporuk and Raible, 2008; Aman and Piotrowski, 2009).

Teeth are unique to vertebrates and have played a central role during evolution. Tooth position, number, shape, and size vary significantly among species, and this diversity is driven by natural selection in response to the environmental pressures provided by various types of food. The fossil record consists largely of teeth, and the dental features in these remnants have provided most of the information used for analysis of extinct vertebrate species. Thus, understanding the positioning of teeth is important both for developmental and evolutionary biologists. In terms of function, proper tooth positioning is required to ensure correct occlusion and feeding and, therefore, this is likely to be regulated by conserved biological mechanisms that are under evolutionary pressures.

Teeth, like many other organs, initiate their development when the epithelium invaginates into the underlying mesenchyme to form a placode (Jernvall and Thesleff, 2000; Pispa and Thesleff, 2003; Tucker and Sharpe, 2004; Neubüser et al., 1997). The placode then forms a cylindrical invaginated epithelial structure called the dental lamina that is anteroposteriorly oriented along the length of the mandible. In mouse embryos, the dental lamina is evident by embryonic day (E)12.5. The lamina progressively expands to give rise to epithelial buds that will form a more mature tooth primordium. While much work has been done to probe the molecular basis of epithelial-mesenchymal interactions during tooth development (Jernvall and Thesleff, 2000; Pispa and Thesleff, 2003; Tucker and Sharpe, 2004; Neubüser et al., 1997), relatively little is known about the intraepithelial interactions and cellular processes that drive the earliest phases of this process.

The initiation of tooth development in the molar region of the mouse jaw occurs around E11.5, and expression of *Fgf8* in the proximal mandible adjacent to the forming jaw joint is one of the first markers of this process (Neubüser et al., 1997) (Figures 1A, 1D, and 1G). This domain of *Fgf8* expression is transient and disappears by E12.5 (Figures 1B–1I). Although a role for FGF8 signaling in positioning of the mouse molar was previously

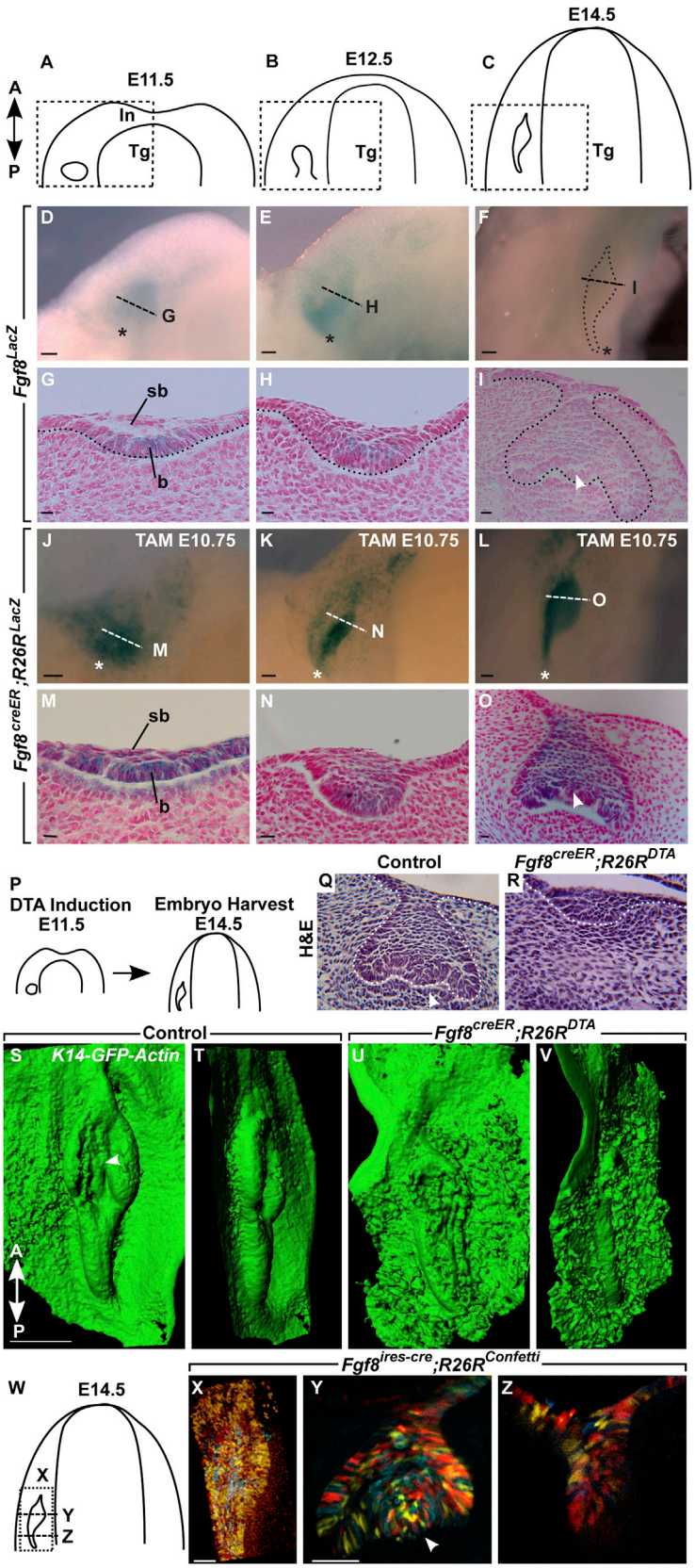

Figure 1. *Fgf8*-Expressing Cells Are Required for Tooth Development

(A–C) Schematic cartoon of early embryonic tooth development showing presumptive dental epithelium at E11.5 (A), dental lamina formation at E12.5 (B), and first molar cap stage at E14.5 (C).

(D–F) $Fgf8^{LacZ}$ was used to visualize *Fgf8* expression during early tooth development (dashed lines represent plane of section for G–I); tongues were removed for clarity. *Fgf8* is expressed at the proximal end of the E11.5 mandible (D) near the anlage of the temporo-mandibular joint (asterisk). The *Fgf8* expression diminishes by E12.5 (E) and is undetectable at E14.5 (F).

(G–I) At E11.5, *Fgf8* is expressed in the basal cell layer (b) of epithelium, but not in the suprabasal layer (sb). At E12.5, *Fgf8* expression diminishes, and it is not detectable at E14.5.

(J–O) Lineage tracing experiments using inducible $Fgf8^{creER}$;$R26R^{LacZ}$. At E11.5, the placode is labeled (J and M), and by E12.5, progeny of *Fgf8*-expressing cells are concentrated in the dental lamina (K and N). At E14.5, the entire molar tooth germ is comprised of descendants of *Fgf8*-expressing cells (L and O).

(P) Experimental scheme for ablation of *Fgf8*-expressing cells.

(Q and R) H&E-stained histological sections of E14.5 molar area from control (Q) and ablated embryo (R). The ablation of *Fgf8*-positive cells blocks tooth germ growth, but does not alter epithelial integrity nor perturb epithelial invagination, indicating that descendants of *Fgf8*-expressing cells are essential for dental epithelium growth, but not for initiation of invagination.

(S–V) 3D reconstructions rendered from confocal optical sections through molar area in control (S and T) and ablated embryo (U and V).

(W–Z) Analysis of $Fgf8^{ires\text{-}cre}$;$R26R^{Confetti}$ embryo to determine distribution of tooth germ epithelial cells at E14.5. The whole mount image (X) and frontal sections (Y and Z) of E14.5 molar show mosaic organization of *Fgf8*-expressing cell progeny.

The white arrowhead in (I), (O), (Q), (S), and (Y) points to the enamel knot (incisors = In and tongue = Tg). The scale bars in (D)–(F), (J)–(L), (S)–(V), (Y), and (Z) represent 100 μm and (G)–(I) and (M)–(O) represent 10 μm.

See also Figure S1 and Movie S1.

suggested (Neubüser et al., 1997), how the precise position of the tooth germ is achieved has remained unknown.

RESULTS

To understand the initial events in tooth development, we first set out to identify the progeny of the *Fgf8*-expressing cells. We performed lineage tracing in $Fgf8^{creER};R26R^{LacZ}$ embryos, in which cre recombination activity depends on induction with tamoxifen. Activation of cre-mediated expression of *LacZ* before E11.5, followed by analysis at E11.5–E14.5, led to labeling of the majority of tooth epithelial cells (Figures 1J–1O), similar to what we found with use of a constitutive $Fgf8^{ires\text{-}cre}$ driver (Figures S1A–S1F). We further verified these data by analyzing $Fgf8^{creER};R26^{mT/mG}$ embryos, which showed similar patterns of lineage tracing and also highlighted that recombination occurred exclusively in the oral epithelium, but not mesenchyme (Figures S1G–S1I). In contrast, activation of $Fgf8^{creER}$ after ~E11.5 led to labeling of essentially no cells in the tooth germ at E14.5 (Figures S1J–S1L). Thus, the lineage tracing studies demonstrated that the cells expressing *Fgf8* at ~E11.5 give rise to most of the epithelial cells of the developing tooth.

Interestingly, whereas at E11.5, the *Fgf8* progeny were essentially overlapping with the domain of *Fgf8* expression (Figures 1D and 1J), at E12.5, the *Fgf8* progeny were condensed in the anteroposteriorly oriented dental lamina, reaching more anteriorly than the original domain of *Fgf8* expression (Figure 1K). The striking change in the distribution of labeled progeny of the *Fgf8*-expressing cells between E11.5 and E12.5 provided the first clue that a highly dynamic epithelial rearrangement process occurs during initiation of tooth development. We were also surprised to observe that the *Fgf8*-expression domain was distinct from the *Shh*-expressing cells in E11.5 embryos and remained distinct even after formation of the dental lamina at E12.5, suggesting a potential interaction between these two populations of cells (Figures S1S–S1Z).

We next used a toxin-based ablation approach to ask whether the *Fgf8*-expressing population is required for formation of the tooth germ. $Fgf8^{creER}$-driven expression of diphtheria toxin A (DTA) was used to induce cell death in the *Fgf8*-expressing population (Figure 1P). Histological sections and 3D reconstructions of the oral epithelium after DTA-mediated ablation of *Fgf8*-expressing cells showed that only initiation of the early dental epithelium, or lamina, occurred, whereas further growth of the epithelium and budding of the tooth germs did not (Figures 1Q–1V; Movie S1). Thus, descendants of the *Fgf8*-expressing cells are required for dental epithelium growth, and other epithelial cells in the area cannot compensate for the absence of this population to form a tooth germ.

As the lineage tracing and ablation experiments demonstrated the importance of the *Fgf8*-expressing cells for tooth development, we set out to identify the mechanism by which this population contributes to the initiation of the dental lamina and to further tooth development. To further evaluate how the tooth germ forms from the progeny of the *Fgf8*-expressing population, we examined the clonal organization of the descendants of the *Fgf8*-expressing cells by crossing the $Fgf8^{ires\text{-}cre}$ driver with a confetti multicolor reporter. If the clonal pattern were fixed at E11.5, we would expect conspicuous patches of similarly colored cells in the growing molar primordium. However, we observed a highly mosaic distribution of cells within the tooth germ at E14.5 (Figures 1W–1Z), indicating that between E11.5 and E14.5 the descendants of *Fgf8*-expressing cells undergo dynamic rearrangement within the oral epithelium. To determine if this cell rearrangement behavior was specific to early tooth development, we compared the clonal patterns in the tooth to those in the tongue epithelium. We used a $Shh^{EGFP/cre}$ driver to activate the confetti reporter at E11.5 and analyzed tongue epithelium at E14.5 (Figures S1M–S1Q), with the same temporal dosing scheme as for the dental epithelium. The tongue epithelium grew in a much more clonal fashion than did the dental epithelium derived from *Fgf8*-expressing cells (Figure S1R), indicating that the cell rearrangement is a specific property of the tooth epithelium as opposed to a general property seen in all oral epithelia.

To assess how the *Fgf8*-expressing cells were organized at early time points, we analyzed $Fgf8^{ires\text{-}cre};R26R^{Confetti}$ E11.5 mandibles by confocal microscopy (Figures 2A–2E and S2A–S2C). We first observed that cells in paraformaldehyde (PFA)-fixed samples lost their elongated shape and were not organized in an obvious pattern (Figures 2B, 2C, and S2A–S2C). However, in live samples, the cells maintained their elongated shape, had a centripetal orientation, and were arranged in a pattern that resembled a large rosette (Figures 2D and 2E). The sensitivity of this rosette structure to fixation indicates its fragility and may explain why it was not previously discovered. To better visualize the rosette-like structure, we analyzed the expression of E-cadherin by crossing $Ecad^{CFP}$ mice with $Fgf8^{creER};R26R^{RFP}$ reporter mice. Under higher magnification, we observed that the central part of the large rosette-like structure consisted of smaller rosettes resembling the classical rosettes observed during germ-band extension in *Drosophila* (Blankenship et al., 2006), in the zebrafish lateral line (Nechiporuk and Raible, 2008), or during mammalian neuro-epithelial development (Afonso and Henrique, 2006) (Figures S2D and S2E). In addition to visualizing E-cadherin, we also assessed the distribution of actin filaments in the rosette area of the mandible using live imaging of Lifeact mice (Riedl et al., 2010). The actin distribution corresponded to the smaller rosette structures in the center of the region of interest and there was more intense actin distribution in the center (Figure S2F, arrowhead). This pattern of actin distribution suggests that the centripetal orientation in the *Fgf8*-expressing region is maintained through active cell adhesion, which is similar to what has been reported in other developmental models (Harding et al., 2014).

The location of the rosette structure adjacent to the jaw joint at E11.5 corresponded to the center of the *Fgf8*-expressing population at E11.5 (Figures 1D and 1J). Because our initial experiments demonstrated that the distribution of *Fgf8*-expressing cell progeny changes between E11.5 and E12.5, we sought to determine the fate of descendants of *Fgf8*-expressing cells in the rosette by performing time-lapse confocal live imaging of the rosette cells using $Fgf8^{ires\text{-}cre};R26R^{Confetti}$ embryos (Figure 2F). E11.5 mandible explants were submerged in agarose-containing medium and observed by inverted spinning disk confocal microscopy for 14 hr. The rosette structure disappeared within 14 hr of development in vitro, and cells that were released from the rosette subsequently migrated out of this

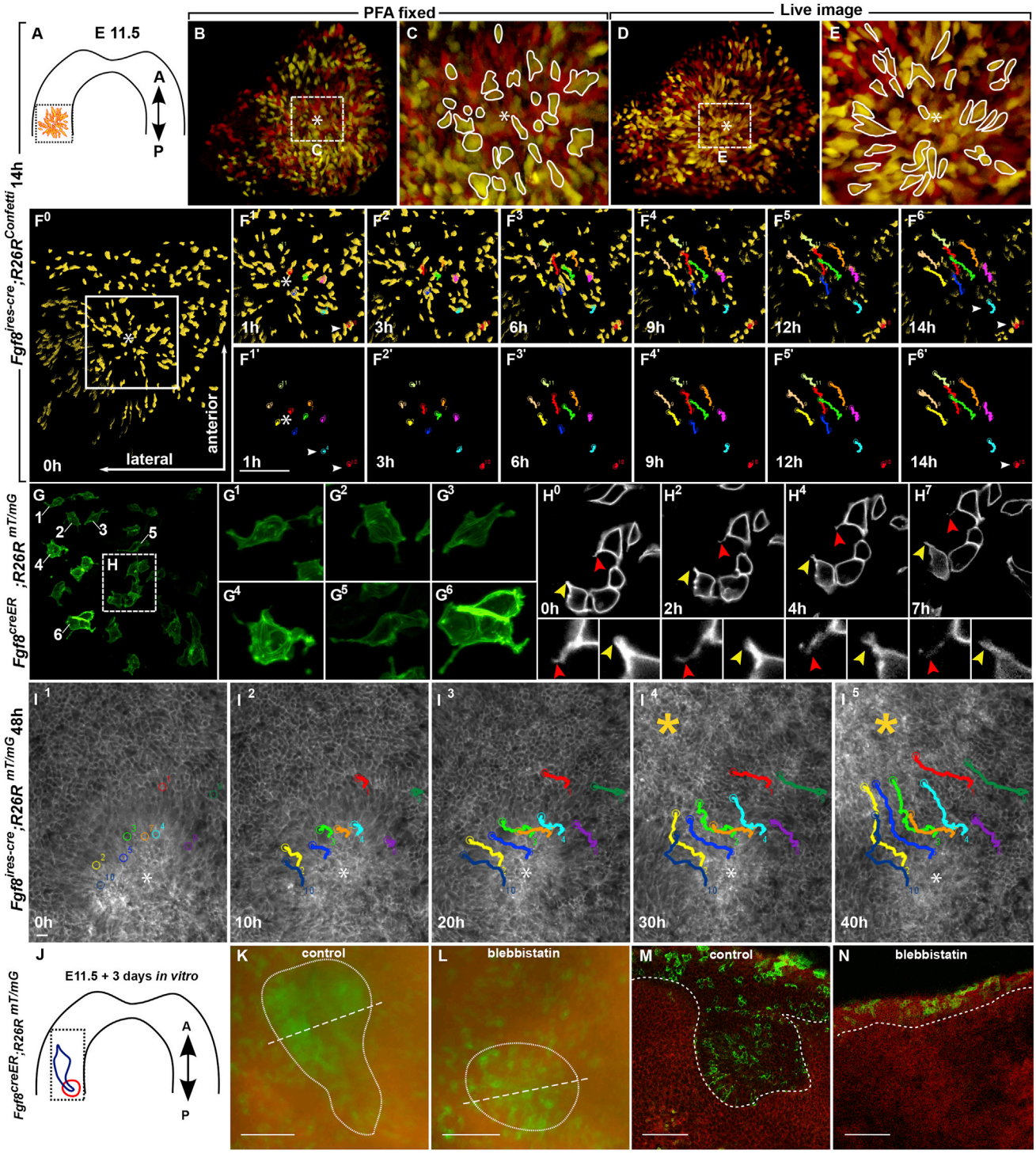

Figure 2. Live Imaging Reveals that *Fgf8*-Expressing Cells Are Organized into a Rosette Structure and Migrate Anteriorly toward the Site of Dental Lamina Initiation

(A) Schematic drawing of *Fgf8*-expressing population at E11.5 (orange structure).

(B–E) Static images of *Fgf8*$^{ires\text{-}cre}$;*R26R*^{Confetti} samples in fixed (B and C) or live (D and E) tissue. The live confocal imaging reveals that the *Fgf8*-expressing population forms a rosette structure as shown in the image.

(F) Confocal time-lapse live imaging shows release of rosette structure during 14 hr of development, as cells from the rosette migrate anteriorly toward the site of dental lamina initiation. The F$^{0'}$– F$^{6'}$ images show tracks to demonstrate the oriented cell movement. The white arrowheads represent the posterior cells that do not move anteriorly.

(legend continued on next page)

region (Figures 2F and S3A–S3C; Movie S2). Cell migration during this period was highly oriented, and cells from the rosette were released and moved in an anterior direction toward the presumptive initiation site of the tooth germ; in contrast, cells located posteriorly from the rosette exhibited minimal movement (Figure 2F, white arrowheads), indicating that the migratory potential was restricted to cells within the rosette area. We next performed automatic cell tracking analysis, which confirmed in an unbiased manner that the migratory behavior was specific to cells in the rosette area and not in cells located posteriorly (Figures S3A–S3C). Interestingly, although the difference in total track length of cell movement was not significant, the difference in cell displacement was highly significant, indicating that cells from the rosette area underwent more directed migration than cells located posteriorly.

We next set out to follow the cell shapes and overall behavior of the cells to determine whether cell migration is an active process specific to the *Fgf8*-expressing population or a result of tissue-level dynamics. We used mosaic labeling of *Fgf8*-expressing cells in *Fgf8*$^{-creER}$;*R26*$^{mT/mG}$ embryos with a lower dose of tamoxifen (2 mg/40 g mouse) in order to induce labeling of individual cells. This experimental design, which enabled us to image individual cells in the posterior mandible, showed that epithelial cells formed fillopodial structures typical of those found in migrating cells (Figure 2G) (Mattila and Lappalainen, 2008). High-magnification time-lapse live imaging revealed that cell movement during migration is accompanied by formation of fillopodial membrane protrusions (Figure 2H, red and yellow arrows; Movie S2).

To complement the mosaic labeling studies, we also analyzed all cells that had expressed *Fgf8* at any point during their developmental history by live imaging of *Fgf8*$^{ires\text{-}cre}$;*R26*$^{mT/mG}$ embryos, in which a membrane GFP labels all descendants of *Fgf8*-expressing cells (Figure 2I). Automated recognition of membrane-labeled cells supported our observation that the directed intraepithelial migration events occurred predominantly in the rosette area (Figures S3D–S3F). As manual tracking was more robust while still allowing us to follow a sufficient number of migrating cells for statistical analysis, we then performed manual tracking of cells in the area of the rosette for a longer period of time. Over a 48 hr period, we observed synchronized cell movement and shape changes of the moving cells as they underwent oriented intraepithelial cell migration toward the area of dental lamina initiation. Interestingly, not only cells from the rosette, but also more anteriorly located descendants of *Fgf8*-expressing cells moved in an oriented fashion toward the site of dental lamina initiation (Figure 2I, yellow asterisk; Movie S2; Figures S3D–S3F).

To test if active epithelial cell migration is required during the initiation of tooth development, we treated cultured embryonic mandibles with blebbistatin, a small molecule inhibitor of non-muscle myosin II that disrupts cell migration (Duxbury et al., 2004). This treatment caused the descendants of *Fgf8*-expressing cells to remain at the site of the rosette structure and prevented anterior migration and tooth germ formation (Figures 2J–2N and S3G–S3K). In addition to the morphological analysis, we assayed expression of several genes important for early tooth development, including *Pitx2*, *Msx1*, *Shh*, *Eda*, *Wnt10b*, and *Bmp4* (Figures S3L–S3W). The failure of tooth development after blebbistatin treatment was supported by the dysregulated expression of *Pitx2* in the dental epithelium, but expression of mesenchymal *Msx1* was unchanged, suggesting that early patterning of the mesenchyme was not altered by blebbistatin treatment. After blebbistatin treatment, genes expressed in early dental epithelium, such as *Shh*, *Wnt10b*, and *Eda*, were not detected or were very weak, suggesting that patterning of tooth development is severely affected by the blockade of cell migration. Similarly, *Bmp4* was not detected in the dental epithelium, but expression in the mesenchyme was unaltered, suggesting again that molecular patterning of the mesenchyme may not require migration of epithelial cells. Together, the live imaging and cultured explant approaches provide the first evidence of intraepithelial cell migration during tooth development. These results explain the change in distribution of progeny of *Fgf8*-expressing cells between E11.5 and E12.5 (Figures 1J and 1K) and also address the question of how the dental lamina is formed almost exclusively from the descendants of *Fgf8*-expressing cells (Figures 1L and 1O).

Importantly, the descendants of *Fgf8*-expressing cells in the rosette area have a unique migration pattern compared to other cells in the mandible (Figures S4A–S4G). Segment analysis of the mandible showed that rosette cells have the longest migration length and total directed displacement (Figure S4C). We compared *Fgf8*-expressing cells with *Sox2*-expressing cells and found that the latter showed very limited migration and had an opposite direction of migration at E11.5 (Figures S4N–S4Q; Movie S3). In addition, the underlying mesenchymal cells, in contrast to the migrating epithelial cells, showed minimal displacement (Figures S4K–S4M). These data are consistent with the notion that migration of proximally located epithelial cells is followed by random intercalation into the prospective dental lamina epithelium, resulting in the mosaic distribution of

(G) Higher magnification (400×) view of *Fgf8*-expressing cells in *Fgf8*^{creER};*R26*$^{mT/mG}$ embryo induced by low dose of tamoxifen. The mosaic activation of cre enabled detailed imaging of individual cells (G^1–G^6), showing formation of cell protrusions and fillopodia during active cell movement.

(H) High-magnification live imaging (7 hr) of individual cell cluster, showing membrane dynamic and fillopodia formation during cell migration. The arrowheads point to the membrane protrusions.

(I) Maximal intensity projection of migration characteristics of cell movement over 48 hr of imaging in an *Fgf8*$^{ires\text{-}cre}$;*R26R*$^{mT/mG}$ embryo. The representative cells were selected for manual tracking to document cell movement toward the region of asterisk in I^4–I^5.

(J–N) Blebbistatin treatment of E11.5 mandible. (J) Schematic drawing of tooth initiation area, with red circle corresponding to the E11.5 rosette and blue line to tooth germ at E14.5. (K) Whole-mount view of *Fgf8*^{creER};*R26*$^{mT/mG}$ embryo mandible explanted at E11.5 and grown for 3 days in vitro, showing normal condensation of the descendants of *Fgf8*-expressing cells in the tooth germ. The dashed line marks the position of the optical section in (M). (L) Inhibition of cell migration with 10 μM blebbistatin in culture medium causes the tooth progenitor cells to remain at the posterior region of the mandible, where the rosette structure formed at E11.5. The dashed line marks the position of the optical section in (N). The prospective dental epithelia are marked by the dotted line.

The scale bars represent in (F) 100 μm; (G) 10 μm; (I) and (J) 100 μm; and (K) and (L) 20 μm.

See also Figures S2, S3, S4, and S5 and Movie S2.

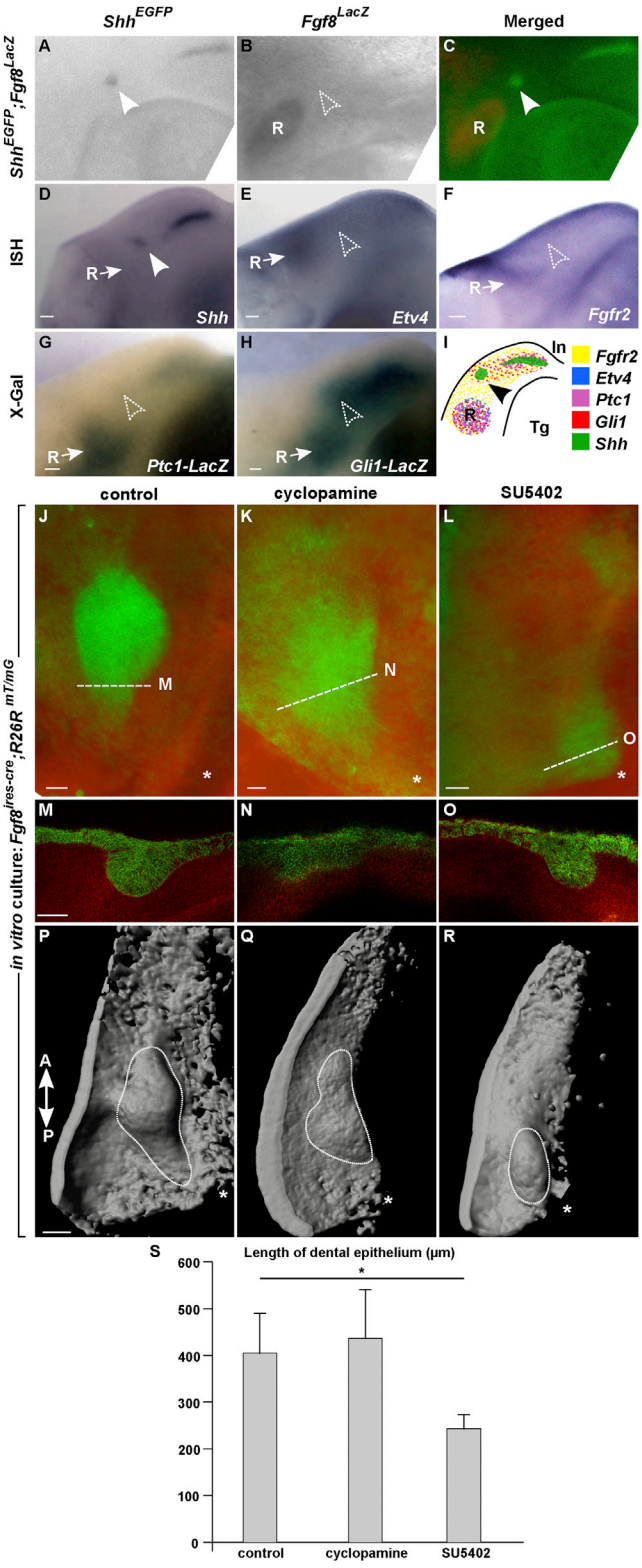

Figure 3. *Fgf8*-Expressing Cells Respond to Both Fgf and Shh Signaling and Do Not Overlap with *Shh* Expression

(A–C) *Shh* and *Fgf8* expression in $Fgf8^{LacZ}$;$Shh^{EGFP/Cre}$ embryonic mandible. The *Shh* expression (arrowhead) is anterior to the *Fgf8*-expressing rosette domain, R.

descendants of *Fgf8*-expressing cells seen at later times in the dental epithelium (Figures 1X–1Z). As the migration pattern suggested coordinated cell movement of epithelial clusters, we examined embryos carrying an E-cadherin-CFP fusion protein ($Ecad^{CFP}$) and found that descendants of *Fgf8*-expressing cells maintained E-cadherin expression and that the intensity of E-cadherin-CFP fluorescence was stronger then between descendants of non-*Fgf8*-expressing cells (Figures S5A–S5D). These findings suggested that the migrating cells preserve cell junctions and support our observation that cells are maintained in epithelial clusters during movement within the oral epithelium.

Next, to identify the signaling mechanism that regulates this cell migration process, we focused on several genes that are expressed at the initiation of tooth development (Dassule and McMahon, 1998; Kettunen et al., 1998). *Shh* is expressed in a small rounded domain (Figures 3A, 3D, and S5E) that has been considered as either the tooth placode (Dassule and McMahon, 1998) or an anterior vestigial structure (Prochazka et al., 2010). We hypothesized that this location of *Shh* expression was anterior to the *Fgf8*-expressing rosette area, and indeed co-expression analysis indicated that the center of the *Fgf8* expression zone was distant from the *Shh*-expressing site of dental lamina initiation at this time (Figures 3B, 3C, and S1T–S1Z). Interestingly, *Etv4,* a readout of Fgf signaling (Roehl and Nüsslein-Volhard, 2001), was expressed at high levels in the rosette area (Figures 3E and S5F), as was the receptor-encoding gene *Fgfr2* (Figures 3F and S5G), indicating that the rosette cells respond to Fgf signals. The Hedgehog receptor *Ptc1* and the downstream Hedgehog target *Gli1* (Dassule and McMahon, 1998; Hardcastle et al., 1998), which are both readouts of Hedgehog (HH) signaling, were also expressed in the rosette area at a distance from the more anterior *Shh*-expressing domain (Figures 3G, 3H, S5H, and S5I), indicating that cells within the rosette were responding to Shh signaling. Thus, these

(D–I) *Fgf8*-positive cells at E11.5 express components of the Fgf and Shh signaling pathways.

(D) *Shh* is expressed in a small anterior rounded domain.

(E and F) *Fgfr2* is expressed throughout the oral epithelium, whereas expression of *Etv4,* a marker of Fgf signaling, is concentrated in the posterior mandible.

(G and H) The HH targets *Ptc1* and *Gli1* are expressed in the rosette.

(I) Summary of expression patterns indicating that *Fgf8*-expressing cells receive both Fgf and Shh signaling (incisor: In and tongue: Tg).

(J–R) Explants of E11.5 $Fgf8^{ires\text{-}cre}$;$R26^{mT/mG}$ embryos cultured for 3 days.

(J, M, and P) Control embryos showing normal tooth bud development in whole mount (J), section (M), and 3D reconstruction (P).

(K, N, and Q) Inhibition of Shh signaling by cyclopamine in cultured explants results in failure of dental epithelium growth, including an ectopic distribution of descendants of $Fgf8^{ires\text{-}cre}$-expressing cells (K), a shallow epithelial invagination (N), and failure of dental epithelial growth, as seen by 3D reconstruction of epithelium (Q).

(L, O, and R) Inhibition of Fgf signaling in explant cultures with SU5402 leads to a small, posteriorly formed bud (L), but invagination of descendants of *Fgf8*-expressing cells is visible in the posterior mandible, presumably at the site of the earlier rosette structure (O and R).

(S) Quantification of anteroposterior length of invaginated dental epithelium in control and after cyclopamine and SU5402 treatment, n = 4 for each condition. The asterisks in (J)–(L) label the position where the jaw joint was cut at the most proximal part of the mandible. A Student's t test was used with SD for error estimates, p = 0.013. The scale bars represent 100 μm.

See also Figure S5.

expression patterns demonstrate that two spatially distinct cell populations are involved in tooth initiation: the *Shh*-expressing cells at the anterior edge of the dental lamina and the posterior rosette cells that express *Fgf8* and are responsive to both Fgf and Shh signaling (Figure 3I).

To test if the Shh and Fgf pathways regulate intraepithelial cell migration from the posterior rosette area into the dental lamina site, we first cultured organ explants from $Fgf8^{ires\text{-}cre}$;$R26R^{mT/mG}$ embryos with inhibitors of Shh (cyclopamine) (Cooper et al., 1998) or Fgf (SU5402) (Mohammadi et al., 1997) signaling for 3 days. Inhibition of Shh signaling prevented condensation of cells after migration, resulting in a more dispersed distribution of descendants of *Fgf8*-positive cells (Figure 3K) compared to control (Figure 3J). Optical sections (Figure 3N) and 3D reconstructions (Figure 3Q) demonstrated that blockade of Shh signaling prevented descendants of *Fgf8*-positive cells from reaching the dental lamina site and hampered formation of the tooth primordium. When the Fgf signaling pathway (Figures 3L, 3O, and 3R) was inhibited, the cells were able to undergo epithelial budding, but strikingly, this occurred in the very posterior part of the mandible, presumably in the original position of the rosette. We also asked if the small molecules were disrupting cell proliferation or induction of apoptosis using EdU pulses to determine the number of proliferative cells and TUNEL staining to quantify apoptosis. These studies showed that neither cyclopamine nor SU5402 caused significant differences in cell proliferation and apoptosis (Figures S5K–S5U).

To address whether the inhibition of Shh and Fgf signaling affects tooth morphogenesis in a cell autonomous manner, we used a genetic approach for ablation of Shh and Fgf8 signaling or overactivation of Shh signaling exclusively in *Fgf8*-expressing cells at E11.5 (Figure 4). Conditional deletion of *Fgf8* led to arrest of cylindrical dental lamina formation (Figure 4B, dotted line), as did conditional deletion of the Shh receptor *Smo* (Figure 4C). In contrast, a *Smo* gain of function allele (*SmoM2*) resulted in an anteriorly expanded dental lamina (Figure 4D), suggesting that Fgf and Shh signaling regulate migration of progenitor cells in a cell autonomous manner during dental lamina formation. Further development of the dental primordium was also affected by deletion of *Fgf8* in progenitor cells (Figure 4F) and resulted in a shorter invaginated structure, similar to what we observed after SU5402 treatment (Figures 3L, 3O, and 3R). Surprisingly, the phenotype in the *Smo* deletion mutants showed some recovery at E14.5 (Figure 4G), suggesting that at later stages other signaling pathways might compensate for the absence of Shh signaling. To link the morphologic phenotypes with cell migration patterns, we performed live imaging experiments followed by analysis of cell migration tracks, displacement, and straightness of movement (Figures 4I–4R; Movie S4). These data show that conditional removal of *Fgf8* led to a dramatic decrease in cell motility, which can explain the missing dental lamina and subsequent defect in positioning of the tooth primordium in *Fgf8* conditional knockout embryos, and they are also consistent with abnormal positioning of the tooth primordium after SU5402 treatment. Deletion of epithelial *Smo* led to decreased length of the invaginated dental lamina accompanied by an increase in cell motility and misorientation of direction of movement (Figure 4O), which was consistent with the in vitro HH blockade using cyclopamine. However, in contrast to the culture experiments, we observed a rescue of tooth development at later stages, suggesting that pharmacological inhibition of HH signaling also affects Shh signaling to the underlying mesenchyme, and this in turn could regulate an alternative signal promoting migration in the prospective dental lamina. Interestingly, *Wnt10b* shows a similar temporospatial expression pattern to *Shh* (Figure S5J) and is involved in regulation of epithelial migration in other systems (Chen et al., 2008). Additionally, we noted that while conditional overactivation of HH signaling resulted in generally lower motility of the *Fgf8*-derived population, a subset of epithelial cells became highly motile, which may contribute to anterior expansion of the dental lamina (Movie S4).

These observations suggested that upregulation of cell migration behavior might lead to anterior expansion of the dental lamina and could cause the additional epithelial budding in the normally toothless area called the diastema seen in some mutants. We therefore performed lineage-tracing experiments with $Fgf8^{creER}$ in *Spry4* null mice (Figures S5V–S5Y), which have been shown (Klein et al., 2006) to have supernumerary teeth in the diastema area in 16% of embryos. We detected formation of a small anterior cap in 38% (n = 8) of $Spry4^{-/-}$; $Fgf8^{creER}$;$R26^{mT/mG}$ triple transgenic mutant embryos, and this was accompanied by an anteriorly extended dental lamina colonized by descendants of the *Fgf8*-expressing population. Thus, the *Fgf8*-expressing cells are not only the source of the first molar epithelium, but also of supernumerary teeth in those mutants that have them.

We next imaged descendants of *Fgf8*-positive cells after inhibition of Shh and Fgf signaling using $Fgf8^{ires\text{-}cre}$;$R26R^{Confetti}$ embryos (Figures 5A–5C; Movies S2 and S4). Each positive cell in the rosette area (Figures 5A–5C) was analyzed to evaluate the length of track and direction of movement (Figures 5D–5L). After inhibition of Shh signaling, *Fgf8* descendants were still able to move in the general direction of the future tooth germ, but this movement was misoriented (Figures 5E, 5H, and 5K; Movie S4). In contrast, Fgf inhibition caused a significant overall decrease in movement, and cells predominantly remained in the rosette area (Figures 5F, 5I, and 5L; Movie S4), consistent with our earlier observation that this treatment led to epithelial bud formation posteriorly at the original site of the rosette. The orientation of migration in the control group differed significantly from both cyclopamine and SU5402 treatment groups in terms of actual and relative vector lengths. Cyclopamine and SU5402 treated explants also differed from each other significantly in terms of vector lengths. In contrast to control samples, in which the cell migration orientation was reproducibly consistent, both cyclopamine and SU5402 treatment caused misoriented cell movement (Figures 5M–5O). However, cyclopamine treated cultures showed a tendency to maintain the direction of migration within the same quadrant as the control, in contrast to SU5402 treatment. This observation suggests that cells in proximity to the prospective dental lamina might secrete an additional chemotactic signal. Lastly, we placed SHH-soaked beads into the posterior side of the explant (opposite to the direction of migration), and the total number of cells accumulated around the bead was quantified (Figures S5Z–S5Zd). Descendants of *Fgf8*-expressing cells accumulated on the surface of SHH-soaked beads after 24 hr of in vitro culture, whereas we did

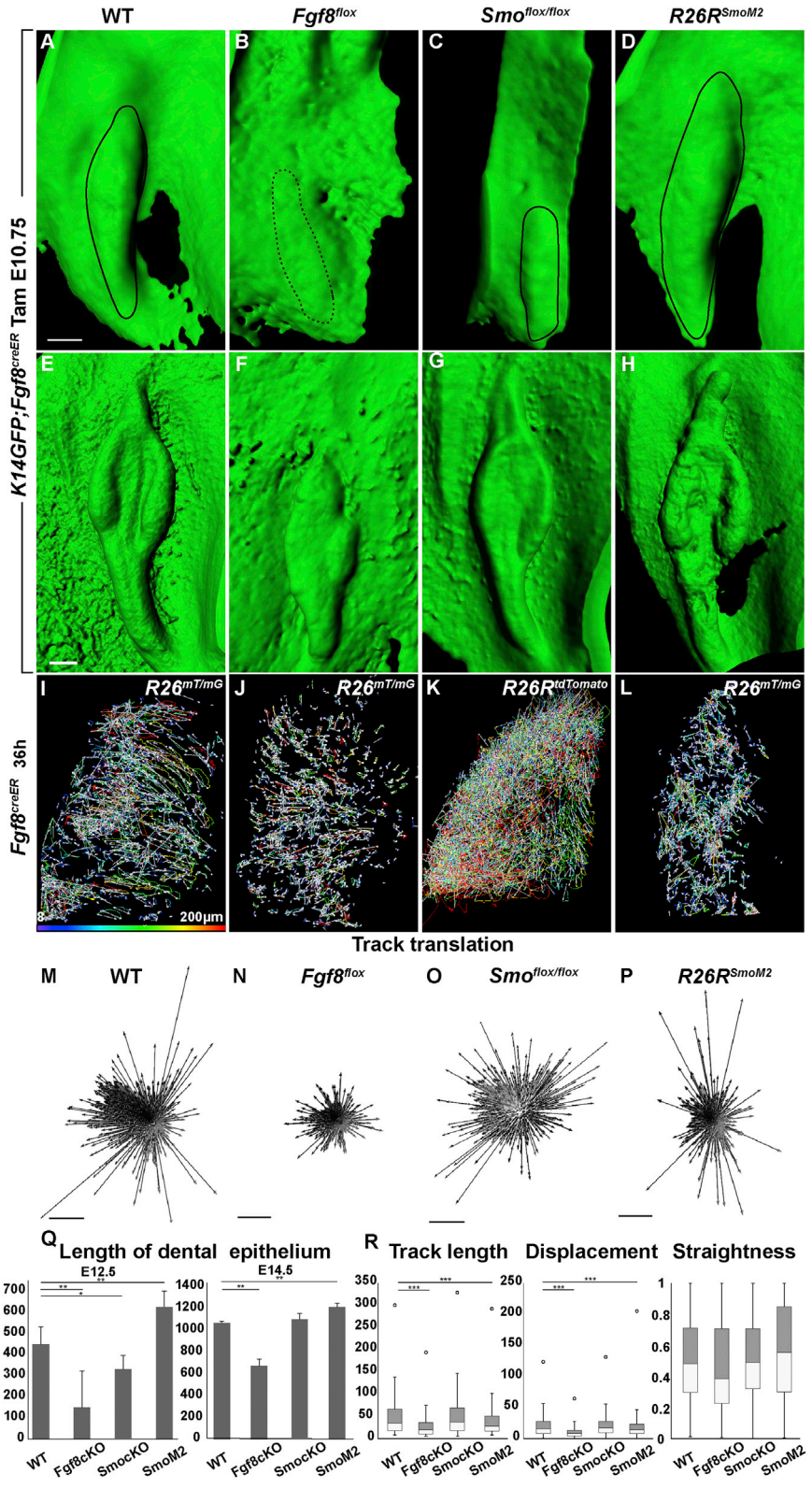

Figure 4. Fgf and Shh Signaling Regulate Migratory Behavior of the Descendants of *Fgf8*-Expressing Epithelial Cells in a Cell-Autonomous Manner

(A–D) Dental lamina formation at E12.5 in Shh and Fgf signaling pathway mutants.

(A) Control (wild-type, WT).

(B) Conditional deletion of *Fgf8* with $Fgf8^{creER}$.

(C) Conditional deletion of *Smo* with $Fgf8^{creER}$.

(D) Conditional gain of function in Shh signaling with SmoM2 allele driven by $Fgf8^{creER}$.

(E–H) First molar tooth germ morphology at E14.5.

(E) Control.

(F) Conditional deletion of *Fgf8*.

(G) Conditional deletion of *Smo*.

(H) Conditional gain of function in Shh signaling.

(I–L) Live imaging with individual cell tracing.

(I) Control.

(J) Conditional deletion of *Fgf8*.

(K) Conditional deletion of *Smo*.

(L) Conditional gain of function in Shh signaling.

(M–P) Track translation analysis of live imaging experiments.

(Q) Quantification of dental lamina size at E12.5 and first molar primordium length at E14.5.

(R) Quantification of cell migration parameters (track length, displacement, and straightness). SD was used for error estimates in column graphs, the box plots are presented with end of whiskers set at the 1.5× interquartile range above the third quartile and below the first quartile; and the open circles mark maximal outliers (Student's t test with * = $p < 0.05$; ** = $p < 0.01$; and *** = $p < 0.0001$). See also Movie S4.

DISCUSSION

Together, the expression, ablation, live imaging, genetic, and inhibitor studies suggest a model in which the tooth bud initiates with a small group of *Shh*-expressing cells, and these in turn recruit a much larger cohort of *Fgf8*-expressing cells that are required for further development (Figure 5P). Our data indicate that the induction of tooth development, which has been generally believed to involve *Shh*-expressing cells in the epithelium interacting with cells in the underlying mesenchyme, results from more complex events than previously thought. The earliest inductive interactions include those between two epithelial populations in addition to the known epithelial-mesenchymal communication. Intraepithelial migration of founder epithelial cells during the early positioning of organs provides an important link between expression patterns of signaling molecules and cellular processes driving early organogenesis. These signaling molecules do not simply act on static populations of progenitors, but rather instruct the location at which the progenitors begin to

not observe a similar pattern with control BSA soaked beads, demonstrating that SHH can indeed function as a chemotactic signal in the developing mandible.

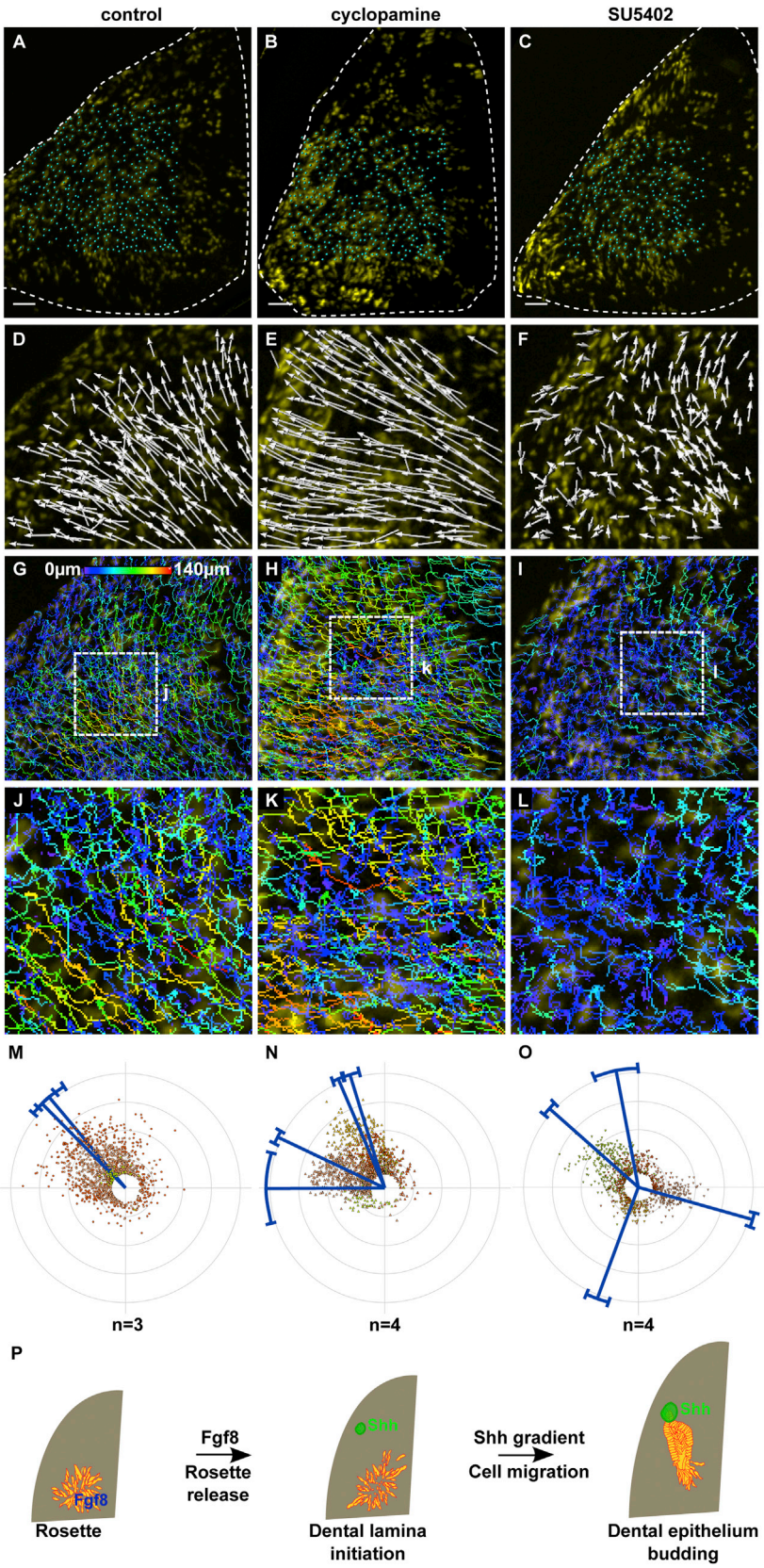

Figure 5. Direction of Cell Migration Is Regulated by Fgf and Shh Signaling

(A–L) Maximal intensity projection of live imaging of mandibles from *Fgf8*$^{ires\text{-}cre}$;*R26R*^{Confetti} embryos to analyze the effects of inhibition of Shh and Fgf signaling on directionality of cell migration.

(A–C) Tracked cells were automatically recognized (cyan points) and followed for 30 hr.

(D–F) Vector replacement to visualize direction of cell movement. In controls, the longest vectors were from the rosette area, whereas in cyclopamine treated mandibles (E), there was no difference in vector length between rosette and non-rosette cells, and rosette vectors were misoriented. In the SU5402 treated mandibles (F), the vector length was decreased.

(G–I) Tracks of individual cells showing displacement as visualized by trajectories of individual cell movement. The cold colors (blue/green) indicate shorter paths and the warm colors (red/yellow) indicate longer paths. In each image, the box is centered on the rosette structure.

(J–L) Detailed view of cell trajectories within the rosette, showing that in the control sample (J), the longest trajectories were from cells in the rosette area, but in cyclopamine treated mandibles (K), the longest trajectories were distributed randomly, and in SU5402 treated mandibles, the cell movement trajectories were minimal.

(M–O) Quantification of cell migration. Each blue line represents an individual experiment, and the dots are individual cells from all experiments. An analysis of three control samples and four experimental samples showed a significant difference among experimental conditions. The orientation of cell migration in the control group differed significantly from both cyclopamine and SU5402 treatment groups in terms of actual ($F = 16.909$, $p < 0.0001$ and $F = 171.423$, $p < 0.0001$) and relative ($F = 32.917$, $p < 0.0001$ and $F = 158.461$, $p < 0.0001$) vector lengths. The cyclopamine and SU5402 treated explants also differed from each other significantly in terms of vector lengths and direction ($F = 319.667$, $p < 0.0001$ and $F = 336.234$, $p < 0.0001$). To compute the circular statistics, we used Oriana 4 and Hotelling's two-sample test with Bonferroni's correction was used for testing differences between treatment groups.

(P) Model for roles of Fgf8 and Shh signaling in regulation of epithelial cell migration. The scale bars represent 100 μm.

See also Figure S5 and Movie S4.

execute their developmental programs. Directional migration within the epithelial layer of a founder population of tooth cells in response to a signaling stimulus provides a new mechanism for the translation of molecular patterning information into cellular behaviors during odontogenesis.

The observation of migratory behavior in the tooth epithelial founder cells leads us to pose an evolutionary question: might this phenomenon, first identified during mouse molar initiation, be a more general feature of mammalian tooth development, and if so, what evolutionary implications might this have? Although tooth developmental programs and the molecular pathways that regulate them appear conserved among species (Jernvall and Thesleff, 2000; Buchtová et al., 2008; Fraser et al., 2009; Smith et al., 2009), tooth positioning and jaw morphology are highly variable in vertebrates. It has been proposed that teeth have a high degree of independence from jaw bone elements both developmentally and evolutionarily, and that tooth induction sites could be at the posterior areas of the jaw in close proximity to the buccopharyngeal membrane or the sites of jaw joints (Smith, 2003; Fraser and Smith, 2011). Thus, one hypothesis that emerges from this work is that migration of founder cells might confer plasticity on tooth positioning despite tight conservation of the tooth initiation process, which would enable greater diversity in pharyngeal arch morphology.

Another evolutionary notion raised by this work relates to the observation in axolotls that posteriorly located epithelium, presumably from the dissolving buccopharyngeal membrane of partly endodermal origin, gives rise to teeth (Soukup et al., 2008). Interestingly, some axolotl teeth showed a very high mosaicism between ectodermal and endodermal lineages (Soukup et al., 2008). These data lead us to propose that, in primitive amphibian dentition, we would expect to find epithelial rearrangements and likely intraepithelial migration during early events such as tooth initiation and positioning. Although future studies will be required to determine whether *Fgf8*-expressing founder cells are induced by proximity to cells of endodermal lineage or to signaling from the jaw joint area, we hypothesize that the site of induction of tooth epithelial founder cells might be conserved among different species despite morphological changes throughout evolution. The migration of progenitor cells may be a mechanism functionally linking conserved sites of tooth induction, with the final position of mature teeth reflecting the morphological changes of the bone apparatus during evolution.

Our data build on recent work studying the migration of epithelial cells during development of mammals, including cell displacement during mammary gland morphogenesis (Ewald et al., 2012), sheet migration during eyelid closure (Heller et al., 2014), and centripetal cell compaction during hair placode formation (Ahtiainen et al., 2014). The findings reported here provide an example in which directed intraepithelial migration is a principle mechanism that regulates positioning of a developing organ during mammalian embryogenesis. In other contexts, such as during migration of epithelial cell in the fish lateral line (David et al., 2002; Haas and Gilmour, 2006; Nechiporuk and Raible, 2008; Aman and Piotrowski, 2009) or in invasive carcinomas (Friedl et al., 1995; Nabeshima et al., 1999; Friedl and Gilmour, 2009; Nguyen-Ngoc et al., 2012; Cheung et al., 2013; Theveneau and Mayor, 2013), the migration of epithelial cells is a collective process, as each cell influences its neighbor and makes the migration more efficient. Evidence is mounting that collectiveness of cell migration can be directly regulated by Fgf signaling (Dalle Nogare et al., 2014; Attia et al., 2015; Lebreton and Casanova, 2015), suggesting that the autocrine FGF8 signaling in a subgroup of epithelial cells that we observed may point to collective migration in the tooth founder population. Future studies will be required to investigate if the migratory behavior that we have observed in the tooth meets the formal definition of collective cell migration.

In addition to the evolutionary implications, the intraepithelial migration of tooth founder cells represents a model for studying epithelial cell migration under physiological conditions in mammals, which is important because epithelial cell migration also occurs during tumor formation and expansion in humans. Tumor epithelial cells can collectively invade neighboring tissue without undergoing epithelial-mesenchymal transition (Nabeshima et al., 1999; Friedl and Gilmour, 2009; Cheung et al., 2013), and it is possible that migration of founder epithelial cells during embryonic development shares some properties with invasive epithelial tumor cells. Thus, studying migrating progenitor cells during development can improve our understanding of diverse mechanisms, including the triggering of migratory behavior in epithelial cells, regulation of cell attraction, and intercalation into existing tissues.

EXPERIMENTAL PROCEDURES

Mouse Breeding

All mouse work was performed in accordance with the UCSF Institutional Animal Care and Use Committee. Details about alleles and breeding are provided in the Supplemental Information.

Cell Ablation

Cell ablation was performed as previously described (Wu et al., 2006) using an *Fgf8*^{creER} driver. Tamoxifen was administered at E10.75 to achieve recombination by E11, when the rosette structure is formed. There were six embryos from three females that were analyzed.

In Vitro Culture and Live Imaging

E11.5 embryonic mandibles were dissected and cultured in 0.3% low melting point agarose medium (Prochazka et al., 2010). The dissection was performed to release the mandible from the jaw joint in a reproducible fashion, so that the posterior (distal) border serves as a stable landmark for all dissected mandibles. After dissection of the mandible, the tongue primordium was removed and a single cut between incisors was used to split mandible into two halves. For experimental treatment, the final concentration in the culture medium was: SU5402 2.5 μM; cyclopamine 5 μM; and blebbistatin 10 μM. For each experimental treatment and for live imaging studies, three independent samples were analyzed. The SHH soaked beads were prepared by incubation in 100 ng/μl of recombinant SHH from mammalian cells (StemRD), and control beads were soaked in BSA. There were four explant cultures that were used for each condition. The number of cells adjacent to the bead surface was counted in ImageJ at t0 and after 24 hr. The difference in cell number was statistically evaluated (Student's t test) for SHH and BSA soaked beads. For live imaging, cultures were placed in sealed glass-bottom dishes to avoid evaporation (MatTek) and imaged on a Borealis-modified Yokogawa CSU-X1 spinning disk confocal unit on an inverted Nikon TI microscope stand using a 10× objective (Stehbens et al., 2012).

Imaging Analysis Software

The raw data from live imaging experiments were post processed using Bitplane Imaris software for automatized selection of labeled cells in the region of interest and tracking analysis. Clonal analysis was done by segmentation of single color patches with semiautomatic counting of cells in every color patch

in ImageJ. Clonal behavior was statistically evaluated by a Mann-Whitney unpaired, non-parametric test. Cell migration vector coordinates were exported in XLS files for further statistical analysis. Imaris software was used to render 3D reconstructions from optical sections. Individual cell tracking was done by MTrackJ plugin in ImageJ (Meijering et al., 2012). All quantification data sets are available in Table S1.

Statistical Analysis of Cell Migration

We used four samples for each of two treatment groups (cyclopamine and SU5402) and three control samples with a total number of 16,802 recorded cells. In our experimental design, all three treatments were located on one multiwell plate at once, oriented in the same direction and imaged simultaneously. The orientation of individual 4D data sets was afterward refined in Imaris. Thus, we were able to create mixed groups later for the purposes of analysis (see below), because possible side effects of different orientations of plates under the microscope were constant for all three treatments. The cells were automatically recognized by ImarisTrack module and vector length and displacement in Cartesian coordinates were recorded for each of the cells. To calculate exact orientation of the vector, the following characterization of right triangle was used: $\alpha = \arcsin(|a| / c)$, where α is the orientation angle, $|a|$ is absolute value of the change in one of the axes, and c is the vector length.

We reduced the total number of cells in our analysis, taking only cells from the upper quartile of vector lengths (longer than 25.177 μm), for the following reasons: (1) lowering cell number lowered the power of the test, as a high number of observations can make even slight differences significant, (2) to eliminate most non-migrating cells with the highest probability of short and random vector direction, and (3) to put greater weight on specimens with longer vectors in analysis. The total number of cells analyzed was 3,774 (1,365 for control, 1,399 for cyclopamine, and 1,010 for SU5402).

To compute circular statistics, we used Oriana 4 (Kovach, 2011). Because the nested analysis required by the experimental design is not an available method for circular statistics, we created mixed groups for each of the three treatments. Moreover, we computed two series of tests with real as well as constant vector lengths to overcome possible changes in vectors due to different rotation of plates under the camera. The Hotelling's two-sample test was used for testing differences between treatment groups. The basic significance level was set to 0.01 because of the large number of recorded cells and reduced to 0.005 using Bonferroni's correction as the same data were used twice in the same test. All quantification data sets are available in Table S1.

SUPPLEMENTAL INFORMATION

Supplemental Information includes Supplemental Experimental Procedures, five figures, one table, and four movies and can be found with this article online at http://dx.doi.org/10.1016/j.devcel.2015.11.025.

AUTHOR CONTRIBUTIONS

J.P. and O.D.K. planned the studies and wrote the manuscript. Experiments were performed by J.P., M.P., W.D., and J.T., who analyzed the data together with F.S. and R.S. *Fgf8*^{creER} mice were produced by R.H. and J.L.R. and *Fgf8*$^{ires\text{-}cre}$ mice by T.S. All authors discussed the data and revised the manuscript.

CONFLICTS OF INTEREST

The authors declare that they have no competing financial interests.

ACKNOWLEDGMENTS

We are grateful to Jeremy Green and Eleni Panousopoulou, as well as members of the Klein laboratory, for helpful discussions. This work was funded by the following grants from the NIH: R01-DE021420 and R01-DE024988 (to O.D.K.), F32-MH081431 (to R.H.), R01-NS34661 (to J.L.R.), and S10-RR026758 (to T.W.); by funds from Weston Havens Foundation; and by the Academy of Sciences of the Czech Republic (RVO 68378050) and BIOCEV–Biotechnology and Biomedicine Center of the Academy of Sciences and Charles University (CZ.1.05/1.1.00/02.0109).

Received: June 8, 2015
Revised: October 19, 2015
Accepted: November 24, 2015
Published: December 21, 2015

REFERENCES

Afonso, C., and Henrique, D. (2006). PAR3 acts as a molecular organizer to define the apical domain of chick neuroepithelial cells. J. Cell Sci. *119*, 4293–4304.

Ahtiainen, L., Lefebvre, S., Lindfors, P.H., Renvoisé, E., Shirokova, V., Vartiainen, M.K., Thesleff, I., and Mikkola, M.L. (2014). Directional cell migration, but not proliferation, drives hair placode morphogenesis. Dev. Cell *28*, 588–602.

Aman, A., and Piotrowski, T. (2009). Multiple signaling interactions coordinate collective cell migration of the posterior lateral line primordium. Cell Adhes. Migr. *3*, 365–368.

Attia, L., Schneider, J., Yelin, R., and Schultheiss, T.M. (2015). Collective cell migration of the nephric duct requires FGF signaling. Dev. Dyn. *244*, 157–167.

Blankenship, J.T., Backovic, S.T., Sanny, J.S.P., Weitz, O., and Zallen, J.A. (2006). Multicellular rosette formation links planar cell polarity to tissue morphogenesis. Dev. Cell *11*, 459–470.

Buchtová, M., Handrigan, G.R., Tucker, A.S., Lozanoff, S., Town, L., Fu, K., Diewert, V.M., Wicking, C., and Richman, J.M. (2008). Initiation and patterning of the snake dentition are dependent on Sonic hedgehog signaling. Dev. Biol. *319*, 132–145.

Chen, K., Fallen, S., Abaan, H.Ö., Hayran, M., Gonzalez, C., Wodajo, F., MacDonald, T., Toretsky, J.A., and Üren, A. (2008). Wnt10b induces chemotaxis of osteosarcoma and correlates with reduced survival. Pediatr. Blood Cancer *51*, 349–355.

Cheung, K.J., Gabrielson, E., Werb, Z., and Ewald, A.J. (2013). Collective invasion in breast cancer requires a conserved basal epithelial program. Cell *155*, 1639–1651.

Cooper, M.K., Porter, J.A., Young, K.E., and Beachy, P.A. (1998). Teratogen-mediated inhibition of target tissue response to Shh signaling. Science *280*, 1603–1607.

Dalle Nogare, D., Somers, K., Rao, S., Matsuda, M., Reichman-Fried, M., Raz, E., and Chitnis, A.B. (2014). Leading and trailing cells cooperate in collective migration of the zebrafish posterior lateral line primordium. Development *141*, 3188–3196.

Dassule, H.R., and McMahon, A.P. (1998). Analysis of epithelial-mesenchymal interactions in the initial morphogenesis of the mammalian tooth. Dev. Biol. *202*, 215–227.

David, N.B., Sapède, D., Saint-Etienne, L., Thisse, C., Thisse, B., Dambly-Chaudière, C., Rosa, F.M., and Ghysen, A. (2002). Molecular basis of cell migration in the fish lateral line: role of the chemokine receptor CXCR4 and of its ligand, SDF1. Proc. Natl. Acad. Sci. USA *99*, 16297–16302.

Duxbury, M.S., Ashley, S.W., and Whang, E.E. (2004). Inhibition of pancreatic adenocarcinoma cellular invasiveness by blebbistatin: a novel myosin II inhibitor. Biochem. Biophys. Res. Commun. *313*, 992–997.

Ewald, A.J., Huebner, R.J., Palsdottir, H., Lee, J.K., Perez, M.J., Jorgens, D.M., Tauscher, A.N., Cheung, K.J., Werb, Z., and Auer, M. (2012). Mammary collective cell migration involves transient loss of epithelial features and individual cell migration within the epithelium. J. Cell Sci. *125*, 2638–2654.

Fraser, G.J., and Smith, M.M. (2011). Evolution of developmental pattern for vertebrate dentitions: an oro-pharyngeal specific mechanism. J. Exp. Zoolog. B Mol. Dev. Evol. *316B*, 99–112.

Fraser, G.J., Hulsey, C.D., Bloomquist, R.F., Uyesugi, K., Manley, N.R., and Streelman, J.T. (2009). An ancient gene network is co-opted for teeth on old and new jaws. PLoS Biol. *7*, e31.

Friedl, P., and Gilmour, D. (2009). Collective cell migration in morphogenesis, regeneration and cancer. Nat. Rev. Mol. Cell Biol. *10*, 445–457.

Friedl, P., Noble, P.B., Walton, P.A., Laird, D.W., Chauvin, P.J., Tabah, R.J., Black, M., and Zänker, K.S. (1995). Migration of coordinated cell clusters in

mesenchymal and epithelial cancer explants in vitro. Cancer Res. *55*, 4557–4560.

Haas, P., and Gilmour, D. (2006). Chemokine signaling mediates self-organizing tissue migration in the zebrafish lateral line. Dev. Cell *10*, 673–680.

Hardcastle, Z., Mo, R., Hui, C.C., and Sharpe, P.T. (1998). The Shh signalling pathway in tooth development: defects in Gli2 and Gli3 mutants. Development *125*, 2803–2811.

Harding, M.J., McGraw, H.F., and Nechiporuk, A. (2014). The roles and regulation of multicellular rosette structures during morphogenesis. Development *141*, 2549–2558.

Heller, E., Kumar, K.V., Grill, S.W., and Fuchs, E. (2014). Forces generated by cell intercalation tow epidermal sheets in mammalian tissue morphogenesis. Dev. Cell *28*, 617–632.

Jernvall, J., and Thesleff, I. (2000). Reiterative signaling and patterning during mammalian tooth morphogenesis. Mech. Dev. *92*, 19–29.

Kettunen, P., Karavanova, I., and Thesleff, I. (1998). Responsiveness of developing dental tissues to fibroblast growth factors: expression of splicing alternatives of FGFR1, -2, -3, and of FGFR4; and stimulation of cell proliferation by FGF-2, -4, -8, and -9. Dev. Genet. *22*, 374–385.

Klein, O.D., Minowada, G., Peterkova, R., Kangas, A., Yu, B.D., Lesot, H., Peterka, M., Jernvall, J., and Martin, G.R. (2006). Sprouty genes control diastema tooth development via bidirectional antagonism of epithelial-mesenchymal FGF signaling. Dev. Cell *11*, 181–190.

Kovach, W.L. (2011). Oriana – Circular Statistics for Windows (Wales: Kovach Computing Services).

Lebreton, G., and Casanova, J. (2015). Ligand-binding and constitutive FGF receptors in single Drosophila tracheal cells: Implications for the role of FGF in collective migration. Dev. Dyn. Published online September 5, 2015. http://dx.doi.org/10.1002/dvdy.24345.

Mattila, P.K., and Lappalainen, P. (2008). Filopodia: molecular architecture and cellular functions. Nat. Rev. Mol. Cell Biol. *9*, 446–454.

Meijering, E., Dzyubachyk, O., and Smal, I. (2012). Methods for cell and particle tracking. Methods Enzymol. *504*, 183–200.

Mohammadi, M., McMahon, G., Sun, L., Tang, C., Hirth, P., Yeh, B.K., Hubbard, S.R., and Schlessinger, J. (1997). Structures of the tyrosine kinase domain of fibroblast growth factor receptor in complex with inhibitors. Science *276*, 955–960.

Nabeshima, K., Inoue, T., Shimao, Y., Kataoka, H., and Koono, M. (1999). Cohort migration of carcinoma cells: differentiated colorectal carcinoma cells move as coherent cell clusters or sheets. Histol. Histopathol. *14*, 1183–1197.

Nechiporuk, A., and Raible, D.W. (2008). FGF-dependent mechanosensory organ patterning in zebrafish. Science *320*, 1774–1777.

Neubüser, A., Peters, H., Balling, R., and Martin, G.R. (1997). Antagonistic interactions between FGF and BMP signaling pathways: a mechanism for positioning the sites of tooth formation. Cell *90*, 247–255.

Nguyen-Ngoc, K.-V., Cheung, K.J., Brenot, A., Shamir, E.R., Gray, R.S., Hines, W.C., Yaswen, P., Werb, Z., and Ewald, A.J. (2012). ECM microenvironment regulates collective migration and local dissemination in normal and malignant mammary epithelium. Proc. Natl. Acad. Sci. USA *109*, E2595–E2604.

Pispa, J., and Thesleff, I. (2003). Mechanisms of ectodermal organogenesis. Dev. Biol. *262*, 195–205.

Prochazka, J., Pantalacci, S., Churava, S., Rothova, M., Lambert, A., Lesot, H., Klein, O., Peterka, M., Laudet, V., and Peterkova, R. (2010). Patterning by heritage in mouse molar row development. Proc. Natl. Acad. Sci. USA *107*, 15497–15502.

Riedl, J., Flynn, K.C., Raducanu, A., Gärtner, F., Beck, G., Bösl, M., Bradke, F., Massberg, S., Aszodi, A., Sixt, M., and Wedlich-Söldner, R. (2010). Lifeact mice for studying F-actin dynamics. Nat. Methods *7*, 168–169.

Roehl, H., and Nüsslein-Volhard, C. (2001). Zebrafish pea3 and erm are general targets of FGF8 signaling. Curr. Biol. *11*, 503–507.

Smith, M.M. (2003). Vertebrate dentitions at the origin of jaws: when and how pattern evolved. Evol. Dev. *5*, 394–413.

Smith, M.M., Fraser, G.J., Chaplin, N., Hobbs, C., and Graham, A. (2009). Reiterative pattern of sonic hedgehog expression in the catshark dentition reveals a phylogenetic template for jawed vertebrates. Proc. Biol. Sci. *276*, 1225–1233.

Soukup, V., Epperlein, H.-H., Horácek, I., and Cerny, R. (2008). Dual epithelial origin of vertebrate oral teeth. Nature *455*, 795–798.

Stehbens, S., Pemble, H., Murrow, L., and Wittmann, T. (2012). Imaging intracellular protein dynamics by spinning disk confocal microscopy. Methods Enzymol. *504*, 293–313.

Theveneau, E., and Mayor, R. (2013). Collective cell migration of epithelial and mesenchymal cells. Cell. Mol. Life Sci. *70*, 3481–3492.

Tucker, A., and Sharpe, P. (2004). The cutting-edge of mammalian development; how the embryo makes teeth. Nat. Rev. Genet. *5*, 499–508.

Wolpert, L. (1969). Positional information and the spatial pattern of cellular differentiation. J. Theor. Biol. *25*, 1–47.

Wu, S., Wu, Y., and Capecchi, M.R. (2006). Motoneurons and oligodendrocytes are sequentially generated from neural stem cells but do not appear to share common lineage-restricted progenitors in vivo. Development *133*, 581–590.